Photochemistry and Photobiology, 2008, 84: 815–818

Rapid Communication

Ultraviolet Resonance Raman Microprobe Spectroscopy of Photosystem II

Jun Chen and Bridgette A. Barry*

School of Chemistry and Biochemistry and the Petit Institute for Bioengineering and Bioscience, Georgia Institute of Technology, Atlanta, GA

Received 17 August 2007, accepted 17 December 2007, DOI: 10.1111/j.1751-1097.2008.00298.x

ABSTRACT

Photosystem II (PSII) carries out photosynthetic oxygen production and is responsible for the maintenance of aerobic, heterotrophic life. In PSII, protein amino acid residues play an important role in the light-driven electron transfer reactions. Here, we describe an approach to enhancing vibrational signals from PSII proteins through ultraviolet resonance Raman (UVRR) and a microprobe jet flow technique. Our work shows that pump-probe UVRR can be used to monitor intermediates during photosynthetic oxygen evolution.

In photosynthesis, photosystem II (PSII) converts light energy into chemical energy and produces oxygen from water. PSII has been extensively investigated as a prototypical enzyme in photosynthesis and photobiology (1). PSII contains light-harvesting pigments, protein subunits and a manganese-containing oxygen-evolving center. Due to the complexity of PSII, elucidation of light-induced energy conversion in PSII is still a challenging research direction. The catalytic role of specific amino acid residues in the production of oxygen is of particular interest.

Raman spectroscopy is a powerful technique in the determination of macromolecular structure in aqueous solutions. However, Raman spectroscopy is challenging in the presence of fluorescence interference, due to the low intrinsic intensity of Raman scattering. In photosynthetic proteins, both near-infrared and visible probe wavelengths excite substantial fluorescence background signals from photosynthetic pigments and generate spectra, which are dominated by chlorophyll and carotenoid vibrational bands (2–4).

To develop a method to monitor protein-derived structural changes with a low fluorescence background, we have combined ultraviolet resonance Raman (UVRR) spectroscopy (5) with a small-volume, jet flow technique. Use of a red pump beam allows control over the charge separated state of PSII. This pump-probe technique will be generally applicable to photosynthetic reaction centers. Pump-probe visible resonance Raman spectroscopy has been used previously to study the quinone acceptors in a photosynthetic reaction center from purple, nonsulfur bacteria (6), and pump-probe UVRR spectroscopy has been used to study the bound retinal chromophore in bacteriorhodopsin (7). To our knowledge, this is the first time that UVRR spectroscopy has been applied to the study of a photosynthetic reaction center.

UVRR, which uses an ultraviolet laser as an excitation source, is expected to resonantly enhance the spectral contributions of aromatic amino acid residues, such as tyrosine and tryptophan. Aromatic amino acids play critical roles in photo-induced charge separation. Perturbations of tryptophan have recently been reported during primary electron transfer in the bacterial reaction center (8). In addition, tyrosine residues are oxidized and reduced during PSII light-driven electron transfer (9). By adopting a spatially displaced, visible pump-UV probe method, the structures of aromatic amino acid intermediates can be probed on the microsecond time scale. The sensitivity of our approach is enhanced by use of a microscope (10), which focuses the excitation beam and collects Raman scattering from the jet flow sample cell, which has a small volume. Use of a high sample flow rate avoids UV probe-induced sample damage.

PSII exhibits absorption in the UV spectral region (Fig. 1). According to its optical absorption properties, we selected three continuous wave (CW) UV laser lines (Fig. 2a) as Raman excitation sources: 325 nm (from a He-Cd laser; KIMMON, Tokyo, Japan), 244 and 229 nm (both were from an intracavity frequency-doubled Ar ion laser; Cambridge LEXEL 95, Fremont, CA). After plasma emission lines were

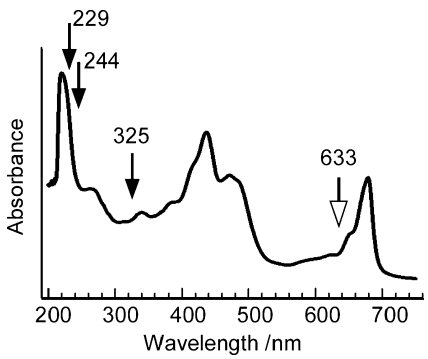

Figure 1. UV–visible absorption spectrum of oxygen-evolving photosystem II. The chlorophyll concentration was 7.7×10^{-3} mg mL^{-1}. The wavelengths marked by solid arrows and the hollow arrow correspond to the wavelengths used as Raman excitation sources and the pump beam, respectively.

*Corresponding author email: bridgette.barry@chemistry.gatech.edu (Bridgette A. Barry)

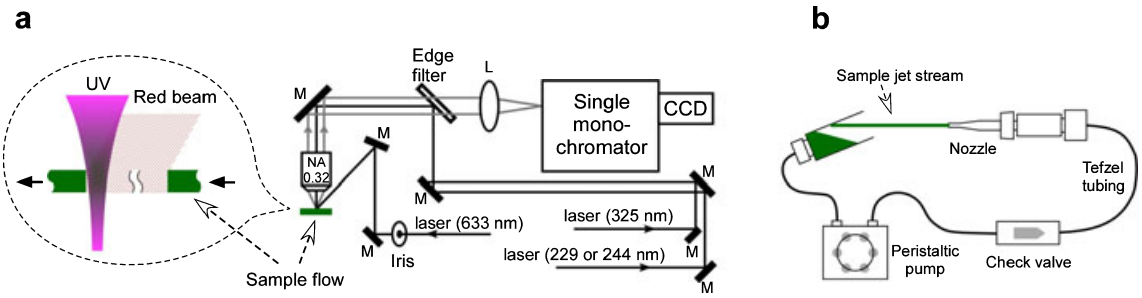

Figure 2. Schematic of (a) the pump-probe UVRR setup (L: lens; M: mirror), and (b) the homemade jet flow sample cell. The incident laser beams and the scattered light are shown as black and gray lines, respectively. At the three different excitation wavelengths, three different edge filters were used to block the Rayleigh scattering. A peristaltic pump with a silicone tubing of inner diameter 2.1 mm was used to force the liquid sample through a homemade nozzle to generate the jet flow, which passed through the red and UV lasers. All these parts were connected by Tefzel tubing (Upchurch Scientific, Inc., Oak Harbor, WA), which is chemically inert and suitable for high pressure applications.

dispersed by a prism and then removed by an aperture, these excitation sources were coupled into a Raman microscope system (Renishaw inVia, Hoffman Estates, IL), which includes a UV objective, edge filters, a single monochromator, and a charge coupled device (CCD) detector. The laser intensity was controlled by a set of neutral density filters. After entering the Raman microscope system, the laser beam was reflected by the edge filter, and defocused on the sample with the UV objective, which was assembled in a Leica microscope. In a backscattering collection mode, Raman scattering from the sample was collected by the UV objective and passed through two edge filters that block Rayleigh scattering. The Raman signal was further focused through a slit in front of the monochromator, which dispersed the light onto a UV-coated, deep-depletion CCD detector. We selected a UV objective (OFR division of Thorlabs, Inc., Caldwell, NJ) with a numerical aperture of 0.32, magnification of 15, an effective focal length of 13 mm, an antireflection coating in the 240–360 nm spectral region and an 8.5 mm working distance. This objective achieves high signal collection efficiency with sufficient space for the jet flow cell. Three sets of wavelength-specific, dielectric edge filters in a rotary mount were individually selected, and their cutoff frequencies were 560, 720 and 500 cm^{-1} for 229, 244 and 325 nm excitation, respectively. In order to reduce the background noise that resulted from scattering light, the width of the slit was fixed at 50 μm, unless otherwise noted. The pixel size was 22 μm, predicting a slit size of 4 pixels with the spectrometer magnification factor of 250 mm/150 mm. The available area of CCD was set to less than 15 pixels (y direction) to reduce readout noise. Prior to the measurement, the spectral linearity was calibrated with the spectrum of acetonitrile, and the accuracy was calibrated with the UV Raman signal of diamond. A 3600 groove/mm holographic grating was used for the dispersion of Raman signal excited by 229 and 244 nm, and a 2400 groove/mm holographic grating was used for 325 nm excitation. The spectral resolutions of the UV Raman measurements were 10, 8 and 6 cm^{-1} for 229, 244 and 325 nm excitation, respectively.

The activity of PSII and possible damage from the UV laser probe beam can be assessed using an oxygen electrode to measure the steady-state rate of O_2 production under illumination (11). UV damage to PSII is expected to interrupt electron transfer, causing a loss of steady-state oxygen-evolving activity. To prevent UV damage, we adopted a flowing sample method (Fig. 2a,b), in which the sample solution was recirculated by a peristaltic pump. For 325 nm excitation, a quartz capillary (300 μm inner diameter) with a flow rate of $\sim$0.8 m s^{-1} was employed. With this method, we acquired a good-quality 325 nm-excited Raman spectrum of PSII (Fig. 3a) with a low fluorescence background. The samples retained oxygen evolution rates of >750 μmol O_2 (mg of chlorophyll)$^{-1}$ h^{-1} after the measurement (Supplemental Materials).

However, the capillary flow rate was too slow to prevent sample damage with 244 and 229 nm excitation in the deep UV. Therefore, we built a jet flow sample cell (Fig. 2b). A quartz nozzle ($\sim$120 μm inner diameter) formed a jet stream

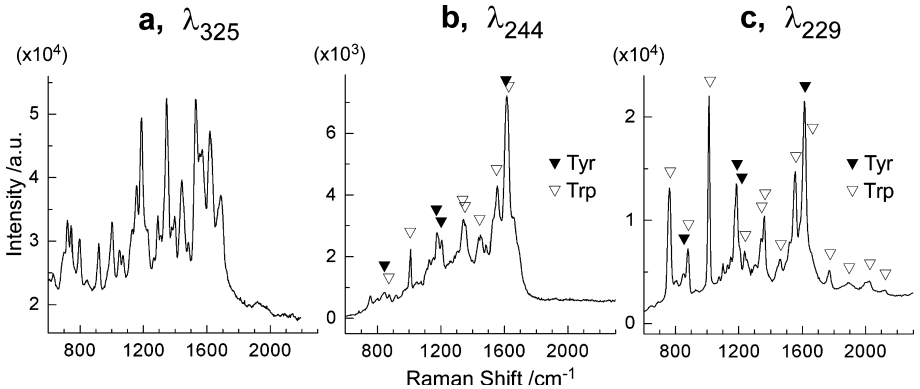

Figure 3. Probe-only UVRR spectra of oxygen-evolving photosystem II excited by (a) 230 μW, 325 nm beam with exposure time of 1.0 h; (b) 560 μW, 244 nm beam with exposure time of 30 min; (c) 560 μW, 229 nm beam with exposure time of 15 min. The chlorophyll concentration was 2.5–2.6 mg mL^{-1} (Supplemental Materials).

with a ~4.5 m s^{-1} flow rate. A nonmetallic check valve (Bio-Chem Valve, Inc., Boonton, NJ) was fixed between the peristaltic pump (GE Healthcare) and the nozzle to improve the quality of the jet stream. The amount of sample required was < 1.0 mL. Using this method, PSII samples retained oxygen evolution rates of > 750 μmol O_2 (mg of chlorophyll)$^{-1}$ h^{-1} after the 244 and 229 nm excited Raman measurements (Fig. 3b,c). We have also tested for spectral artifacts, induced by increasing the 244 nm excitation powers (Fig. S1) or the exposure times (Fig. S2). No significant spectra changes were observed. No white light correction was employed to generate the spectra in Fig. 3.

The UV Raman spectra of PSII samples were recorded at room temperature through the use of the system described above. The reaction center concentration was < 10 μM, as determined from the chlorophyll concentration (Supplemental Materials). Excitation at 325 nm produced a Raman spectrum dominated by vibrational bands from chlorophyll and carotenoid (Fig. 3a), as previously observed with visible and near-infrared excitation wavelengths. However, with 244 and 229 nm excitation, the vibrational signals of tyrosine and tryptophan residues in PSII were selectively enhanced (Fig. 3b,c). The spectral assignments were made using tyrosine and tryptophan vibrational spectrum, recorded from model compounds in solution (12). Furthermore, the oxygen-evolving center and oxidized tyrosine side chains have characteristic electronic transitions in the UV range (13,14) and are expected to be resonantly enhanced at 229 and 244 nm. Therefore, UVRR is a potentially useful technique in the identification of light-induced PSII structural changes.

To explore whether UVRR can be used to study electron transfer intermediates, a visible pump-UV probe experiment must be conducted with a high signal-to-noise ratio. We used a CW 633 nm laser (He-Ne laser; Renishaw RL 633) as a pump beam (Fig. 2a) to induce light-induced charge separation, and 244 nm excitation as the Raman probe. Time resolution can be controlled by adjusting the distance between the pump and the UV laser. In initial experiments, the size of the pump beam was adjusted to a 1.0 mm diameter, with an estimated transit time of 200–250 μs (Fig. 2a). The red pump beam is expected to establish a charge-separated state in the PSII sample. To facilitate generation of this charge-separated state, potassium ferricyanide was added to the PSII sample as an exogenous electron acceptor (15). Reduction of ferricyanide to produce ferrocyanide leads to characteristic changes in the frequency of CN stretching bands (15), which can be used to assess the effect of both pump and probe wavelengths on PSII charge separation. With only the 244 nm probe beam, the vibrational bands of ferrocyanide at 2053 and 2095 cm^{-1} made a negligible contribution to the spectrum (Fig. S3b). However, with the 633 nm pump and the 244 nm probe beams, significant ferrocyanide bands were observed (Fig. S3d). These results demonstrate that there is no significant actinic effect from the 244 nm UV probe.

Figure 4 shows a pump-minus-probe difference UVRR spectrum of PSII, obtained by averaging 10 data sets on ten different samples. The oxygen-evolving complex was removed in the PSII preparations employed (Supplemental Materials). Under these conditions, a redox-active tyrosine Z is the terminal electron donor (9,11), generating a light-induced tyrosyl radical with a lifetime on the hundreds of milliseconds time scale (16). With this 244 nm Raman probe, redox active

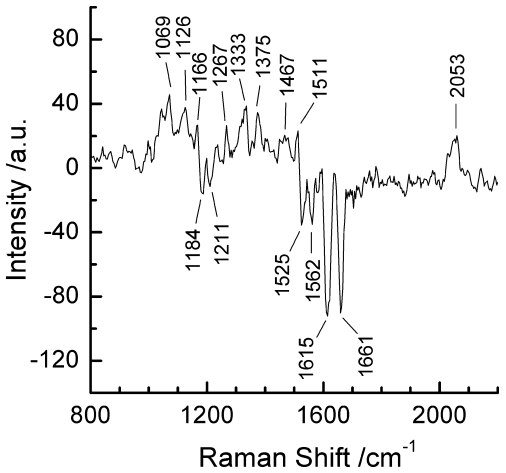

Figure 4. Pump-probe difference UVRR spectrum of photosystem II, from which the oxygen-evolving complex has been removed. The Raman spectrum was obtained by 560 μW, 244 nm beam and an exposure time of 30 min. The polarization of the 244 nm beam was vertical to the sample flow direction. The power of the red pump beam was 11 mW. The difference spectrum represents the average of 10 data sets and was obtained by subtracting the probe-only spectrum from the pump-plus-probe spectrum. The data were acquired with no pixel binning. Three adjacent data points, corresponding to three pixels, were averaged; the 50 μm slitwidth, which contributes to spectral resolution, corresponds to 4 pixels. Potassium ferricyanide (3 mM) was added as an electron acceptor. The chlorophyll concentration was 1.4 mg mL^{-1}.

tyrosine D (9,11), which decays on a much slower time scale (seconds/minutes) and the plastoquinone acceptors, Q_A and Q_B (1,11) are also expected to be detectable. Vibrational bands, which are altered in frequency and intensity by the oxidation (D/Z) or reduction (Q_A/Q_B) reactions will be observed in the difference spectrum. For example, oxidation of tyrosine perturbs ring and CO stretching mode frequencies (17).

In Fig. 4, a red pump-minus-probe difference Raman spectrum, associated with light-induced charge separation, was constructed by subtraction. Unique spectral features of D, Z, Q_A and Q_B will be negative bands; unique spectral features of the radicals will be positive bands. The noise level was reduced to ~10 counts by averaging of three adjacent data points and by signal averaging on multiple samples. The vibrational band at 2053 cm^{-1} in the difference spectrum is attributable to ferrocyanide, which was generated by the light-induced reduction of ferricyanide, indicating that the red pump beam excites a charge separation. In addition, positive bands with frequencies less than 1600 cm^{-1} are exhibited in the difference spectrum (Fig. 4). Moreover, the frequencies of these bands are different from those of tyrosine or tryptophan in Fig. 3b,c. Thus, these bands may be assignable to light-induced intermediates in electron transfer, namely Q_A^-, Q_B^-, tyrosyl radical $Z^{\cdot}$ or tyrosyl radical $D^{\cdot}$. Detailed assignments await isotopic labeling (for one discussion of previous FT-IR assignments, which have been controversial, see Ayala *et al.* [16] and references therein). The negative vibrational band at 1615 cm^{-1} in Fig. 4 may be assignable to the D/Z υ8a ring stretching mode (17). Based on the cyanobacterial PSII crystal structure, there are expected to be ~84 tyrosine residues in a PSII monomer (protein data bank entry 2axt [18]). The total signal intensity at 1615 cm^{-1} is ~7000 counts (data not

shown), so the intensity of the 1615 cm^{-1} band (~80 counts) may be consistent with this spectral feature arising from a single tyrosine. In the presence of ferricyanide, the 244 nm-excited Raman spectrum of oxygen-evolving PSII (Fig. S1) exhibits a vibrational band at 1654 cm^{-1}; however, this band is not present in the 229 nm Raman spectrum (data not shown) or in the 244 nm Raman spectrum obtained in the absence of ferricyanide (Fig. 3b). This comparison suggests that the band at 1654 cm^{-1} is not an amide band, but may originate from plastoquinone. Previous isotopic labeling of PSII plastoquinone has assigned a band at 1659 cm^{-1} to the CO stretch of Q_A (19). Therefore, we favor the assignment of the negative vibrational band at 1661 cm^{-1} in Fig. 4 to Q_A/Q_B.

This work shows that the UVRR microprobe and jet flow techniques can be used to interrogate PSII electron transfer intermediates. The volume of sample required was less than 1.0 mL; sample flow was about 20 s per circulation. Raman probe wavelengths in the deep UV selectively enhanced vibrational signals from tyrosine, tryptophan and electron transfer cofactors. Spectra were acquired at reaction center concentrations of less than 10 μM, and samples retained high levels of activity after the measurement. These results indicate that UVRR will be a useful technique in the study of PSII.

Acknowledgement—This work was supported by National Institutes of Health Grant GM43273 (B.A.B.).

SUPPLEMENTAL MATERIALS

The following supplemental materials are available for this article:

Figure S1. UVRR spectra of oxygen-evolving PSII, with a 510 μW, 244 nm Raman probe beam and an exposure time of 30 min (black) and with a 6.3 mW, 244 nm Raman probe beam with an exposure time of 5 min (red). These spectra were normalized at 1004 cm^{-1}. The slit was set at 60 μm. The chlorophyll concentration was 2.6 mg mL^{-1}, and 3 mM potassium ferricyanide was added to the sample.

Figure S2. UVRR spectra recorded from oxygen-evolving PSII with successive 5 min exposure times. The Raman probe was 6.3 mW at 244 nm. The slit was set at 60 μm. The chlorophyll concentration was 2.6 mg mL^{-1}, and 3 mM potassium ferricyanide was added to the sample.

Figure S3. UVRR spectra of oxygen-evolving PSII showing the red pump-induced reduction of potassium ferricyanide. (a) Ten successive UV probe-only spectra with an exposure time of 3 min each. (b) Sum spectrum of (a). (c) Ten successive red pump-UV probe spectra with a 200–250 μs delay time and an exposure time of 3 min each. (d) Sum spectrum of (c). The UV probe was a 500 μW, 244 nm laser beam. The power of the red pump beam was 11 mW. The chlorophyll concentration was 2.4 mg mL^{-1}, and 3 mM potassium ferricyanide was added to the sample. Spectrum (d) exhibits three vibrational bands at 2053, 2095 and 2132 cm^{-1}. The first two bands with lower frequencies result from ferrocyanide (Suppl. Materials Ref. [6]), which was generated by the reduction of ferricyanide. The vibrational band at 2132 cm^{-1} originates from ferricyanide.

This material is available as part of the online article from: http://www.blackwell-synergy.com/doi/full/10.1111/j.1751-1097.2008.00298.x

Please note: Blackwell Publishing are not responsible for the content or functionality of any supplementary materials supplied by the authors. Any queries (other than missing material) should be directed to the corresponding author for the article.

REFERENCES

1. Nelson, N. and C. F. Yocum (2006) Structure and function of photosystems I and II. *Annu. Rev. Plant Biol.* **57**, 521–565.
2. Shreve, A. P., N. J. Cherepy, S. Franzen, S. G. Boxer and R. A. Mathies (1991) Rapid-flow resonance Raman spectroscopy of bacterial photosynthetic reaction centers. *Proc. Natl Acad. Sci. USA* **88**, 11207–11211.
3. Cua, A., D. H. Stewart, G. W. Brudvig and D. F. Bocian (1998) Selective resonance Raman scattering from chlorophyll Z in photosystem II via excitation into the near-infrared absorption band of the cation. *J. Am. Chem. Soc.* **120**, 4532–4533.
4. Picorel, R., G. Chumanov, E. Torrado, T. M. Cotton and M. Seibert (1998) Surface-enhanced resonance Raman scattering spectroscopy of plant photosystem II reaction centers excited on the red-edge of the Q(y) band. *J. Phys. Chem. B* **102**, 2609–2613.
5. Asher, S. A. (1993) UV resonance Raman-spectroscopy for analytical, physical, and biophysical chemistry. 1. *Anal. Chem.* **65**, A59–A66.
6. Zhao, X., T. Ogura, M. Okamura and T. Kitagawa (1997) Observation of resonance Raman spectra of the semiquinone Q_A^{1-} and Q_B^{1-} in photosynthetic reaction centers from *Rhodobacter sphaeroides R*26. *J. Am. Chem. Soc.* **119**, 5263–5264.
7. Netto, M. M., S. P. Fodor and R. A. Mathies (1990) Ultraviolet resonance Raman spectroscopy of bacteriorhodopsin. *Photochem. Photobiol.* **52**, 605–607.
8. Wang, H., S. Lin, J. P. Allen, J. C. Williams, S. Blankert, C. Laser and N. W. Woodbury (2007) Protein dynamics control the kinetics of initial electron transfer in photosynthesis. *Science* **316**, 747–750.
9. Barry, B. A. and G. T. Babcock (1987) Tyrosine radicals are involved in the photosynthetic oxygen-evolving system. *Proc. Natl Acad. Sci. USA* **84**, 7099–7103.
10. Barry, B. and R. Mathies (1982) Resonance Raman microscopy of rod and cone photoreceptors. *J. Cell Biol.* **94**, 479–482.
11. Barry, B. A. (1995) Tyrosyl radicals in photosystem II. *Methods Enzymol.* **258**, 303–319.
12. Rava, R. P. and T. G. Spiro (1984) Selective enhancement of tyrosine and tryptophan resonance Raman-spectra via ultraviolet-laser excitation. *J. Am. Chem. Soc.* **106**, 4062–4064.
13. Dekker, J. P., J. J. Plijter, L. Ouwehand and H. J. van Gorkom (1984) Kinetics of manganese redox transitions in the oxygen-evolving apparatus of photosynthesis. *Biochim. Biophys. Acta* **767**, 176–179.
14. Gerken, S., K. Brettel, E. Schlodder and H. T. Witt (1988) Optical characterization of the immediate donor to chlorophyll a_{II}^{+} in O_2-evolving photosystem II complexes. *FEBS Lett.* **237**, 69–75.
15. Kim, S. and B. A. Barry (1998) The protein environment surrounding tyrosyl radicals D· and Z· in photosystem II: A difference Fourier-transform infrared spectroscopic study. *Biophys. J.* **74**, 2588–2600.
16. Ayala, I., S. Kim and B. A. Barry (1999) A difference Fourier transform infrared study of tyrosyl radical Z* decay in photosystem II. *Biophys. J.* **77**, 2137–2144.
17. Range, K., I. Ayala, D. York and B. A. Barry (2006) Normal modes of redox-active tyrosine: Conformation dependence and comparison to experiment. *J. Phys. Chem.* **110**, 10970–10981.
18. Loll, B., J. Kern, W. Saenger, A. Zouni and J. Biesiadka (2005) Towards complete cofactor arrangement in the 3.0 Å resolution structure of photosystem II. *Nature* **438**, 1040–1044.
19. Razeghifard, M. R., S. Kim, J. S. Patzlaff, R. S. Hutchison, T. Krick, I. Ayala, J. J. Steenhuis, S. E. Boesch, R. A. Wheeler and B. A. Barry (1999) The *in vivo*, *in vitro*, and calculated vibrational spectra of plastoquinone and the plastosemiquinone anion radical. *J. Phys. Chem. B* **103**, 9790–9800.